Journal of Science: Advanced Materials and Devices 9 (2024) 100773

Contents lists available at ScienceDirect

Journal of Science: Advanced Materials and Devices

journal homepage: www.elsevier.com/locate/jsamd

Research Article

Superconductive and flexible antenna based on a tri-nanocomposite of graphene nanoplatelets, silver, and copper for wearable electronic devices

Ahmed Jamal Abdullah Al-Gburi [a,*], Nor Hadzfizah Mohd Radi [a], Tale Saeidi [b], Naba Jasim Mohammed [c], Zahriladha Zakaria [a], Gouree Shankar Das [d], Akash Buragohain [d], Mohd Muzafar Ismail [a,**]

[a] Center for Telecommunication Research & Innovation (CeTRI), Fakulti Teknologi Dan Kejuruteraan Elektronik Dan Komputer (FTKEK), Jalan Hang Tuah Jaya, 76100, Durian Tunggal, Melaka, Universiti Teknikal Malaysia Melaka (UTeM), Malacca, Malaysia
[b] WiSAR Lab, Atlantic Technological University (ATU), Letterkenny, Co. Donegal, F92 FC93, Ireland
[c] Materials Science Program, Department of Applied Physics, Faculty of Science and Technology, University Kebangsaan Malaysia, Bangi, 43600, Selangor, Malaysia
[d] Microwave Research Laboratory, Department of Physics, Dibrugarh University, Dibrugarh, Assam, 786004, India

ARTICLE INFO

Keywords:
Superconductive
Graphene nanoplatelet/silver/copper (GNP/Ag/Cu)
Flexible antenna
Specific absorption rate (SAR)
Wearable electronics
Scanning electron Microscopy (SEM)

ABSTRACT

Printed electronics, fueled by graphene's conductivity and flexibility, are revolutionizing wearable technology, surpassing copper's limitations in cost, signal quality, size, and environmental impact. Graphene-based inks are positioned to lead in this domain, offering cost-effective solutions directly applicable to materials such as textiles and paper. However, graphene encounters a primary drawback due to its lack of an energy band gap, constraining its potential applications in various electronic devices. In this study, we present a novel formulation of a superconductive, flexible leather graphene antenna utilizing a tri-nanocomposite structure of Graphene Nanoplatelet/Silver/Copper (GNP/Ag/Cu), covering a wideband bandwidth from 5.2 GHz to 8.5 GHz. The electrical conductivity of the GNP/Ag/Cu sample was assessed using the four-point probe method. With each additional layer, conductivity increased from 10.473×10^7 S/m to 40.218×10^7 S/m, demonstrating a direct correlation between conductivity and antenna gain. The study evaluates the efficacy of various thicknesses of conductive Graphene (GNP/Ag/Cu) ink on drill fabric. Safety assurance is provided through specific absorption rate (SAR) testing, indicating 0.84 W/kg per 10 g of tissue for an input power of 0.5 W, in compliance with ICNIRP standards for wearable device safety. Additionally, a morphological analysis of the antenna was conducted, showcasing its potential for efficient signal transmission in wearable electronic devices.

1. Introduction

The rapid advancement in the development of printed conductive inks for electronic applications is driven by their expanding use across various fields such as transistors [1], sensors [2], antennas [3,4], microwave dielectrics [5], wearable electronics [6,7], and graphene based absorbing materials [8]. As the key element in printed electronics, significant efforts have been concentrated on producing highly conductive inks made from metal nanoparticles, particularly silver nanoparticles [9], which are preferred for their superior conductivity and leveling properties. Despite their advantages, the high cost of silver limits its use in budget-sensitive applications [10]. Alternatives like copper and aluminum nanoparticles are more affordable but prone to oxidation, necessitating a sintering process post-printing, which is not viable for heat-sensitive materials like paper or plastic [11,12]. Conductive polymers, another option, can be made into conductive films but tend to be chemically and thermally unstable [13]. Carbon nanotubes were once considered a potential replacement for metal nanoparticles, but their high junction resistance leads to reduced surface conductivity, which restricts their use [14]. Consequently, there is a strong demand within the printed electronics sector for affordable and highly conductive inks.

Antennas play a crucial role in the design of body-centric wireless systems, ensuring reliable power transfer between nodes located on various body parts and facilitating communication with external devices

Peer review under responsibility of Vietnam National University, Hanoi.
* Corresponding author.
** Corresponding author.
E-mail addresses: ahmedjamal@ieee.org, engahmed_jamall@yahoo.com (A.J.A. Al-Gburi), muzafar@utem.edu.my, hadzfizah@umpsa.edu.my (M.M. Ismail).

https://doi.org/10.1016/j.jsamd.2024.100773
Received 24 May 2024; Received in revised form 20 July 2024; Accepted 2 August 2024
Available online 3 August 2024

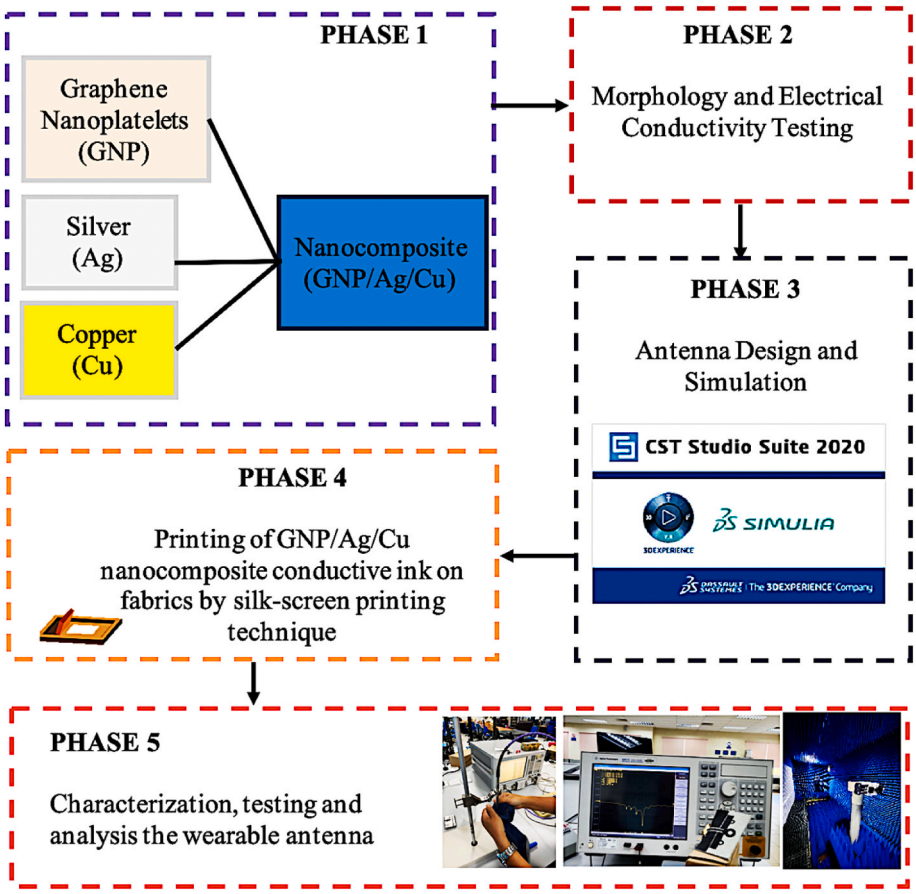

Fig. 1. Illustrates the graphical diagram of the methodological overall process, comprising 5 phases as follows: phase one involves the preparation of GNP/Ag/Cu nanocomposites sample solution. phase two encompasses morphology and electrical conductivity testing. phase three includes antenna design and simulation. phase four involves the printing preparation of GNP/Ag/Cu nanocomposites ink on textile by silk-screen printing. the final phase is dedicated to the characterization and testing of the flexible antenna.

[15]. Wearable communication systems also demand mechanical flexibility and effective radiation, which necessitates the inclusion of passive components such as transmission lines and antennas for transmitting and receiving radio frequency (RF) signals. Consequently, conductive metals, which are readily available and provide reliable solutions, dominate body-centric communication technologies. In textile-based antennas, techniques like embroidery, various printing methods (including inkjet and screen-printing), and patterning of conductive patches have undergone significant study in recent years. Notably, early successful prototypes, such as embroidered antennas [16,17] and microstrip patch antennas [18,19] integrated into textiles, continue to be utilized by modifying their geometries to suit different communication protocols. The application of copper, other conductive foils, and pleated metal threads in creating textile-based antennas has expanded the understanding of textile use in communication. This has led to a design process that accounts for electrical properties and their impact on performance, taking into account factors like the adaptability of textiles to bending, stretching, and compression [20,21]. The focus on developing conformal antenna surfaces specifically for textiles has spurred the innovation of new manufacturing techniques. Common printing techniques, such as inkjet [22] and screen printing [23], have introduced novel production strategies for on-body antenna systems. However, these scalable production options are limited by the vulnerability of the conductive materials to corrosion and oxidation, which also incur high material costs due to performance degradation [24]. Despite these challenges, ongoing research continues to explore various metallic materials, including conductive inks of copper and silver, pleated yarns, and conductive coatings of multiple metals, aiming to enhance the functionality of traditional bulky antennas. Unlike many textile substrates, these metallic antennas require additional protection against water absorption and corrosion.

Carbon nanomaterials, such as graphene, are emerging as superior alternatives to traditional materials due to their exceptional properties like electrical sensitivity, piezoresistivity, high optical transparency, and robustness. Recognizing the demands of the Internet of Things (IoT) for adaptive technologies, graphene has proven effective in wearable applications. Researchers have utilized graphene-based assemblies for developing flexible devices such as gas and chemical sensors, along with wireless strain and tactile sensors. Additionally, there is significant interest in using graphene for creating flexible RFID tags through methods like ink-jet printing [25].

Several articles have been published proposing the use of conductive patches as sheets for wearable applications [26–32]. Groundbreaking efforts by researchers in Ref. [26] led to the development of a reconfigurable antenna based on a metal-hybrid bistable composite tube. This antenna operated at dual-band frequencies of 0.6 and 1.2 GHz and achieved a low gain of 1.8 dBi, limited by the deoxidized metals used. The most recent study [27] presented graphene oxide nanocomposites for highly electrical conductivity measurements in wearable applications. This antenna exhibited a high conductivity of approximately 21.3 $\times$ 10^7 S/m and operated at 2.45 GHz. Tang et al. [28] introduced a highly sensitive wearable sensor based on a flexible multi-layer graphene film antenna. Operating at 1.63 GHz, the antenna achieved a conductivity of 10^6 S/m, and its bending properties were examined to validate its flexibility. An ultra-high conductivity graphene-based flexible antenna was proposed by Scidà et al. [29], offering a conductivity of

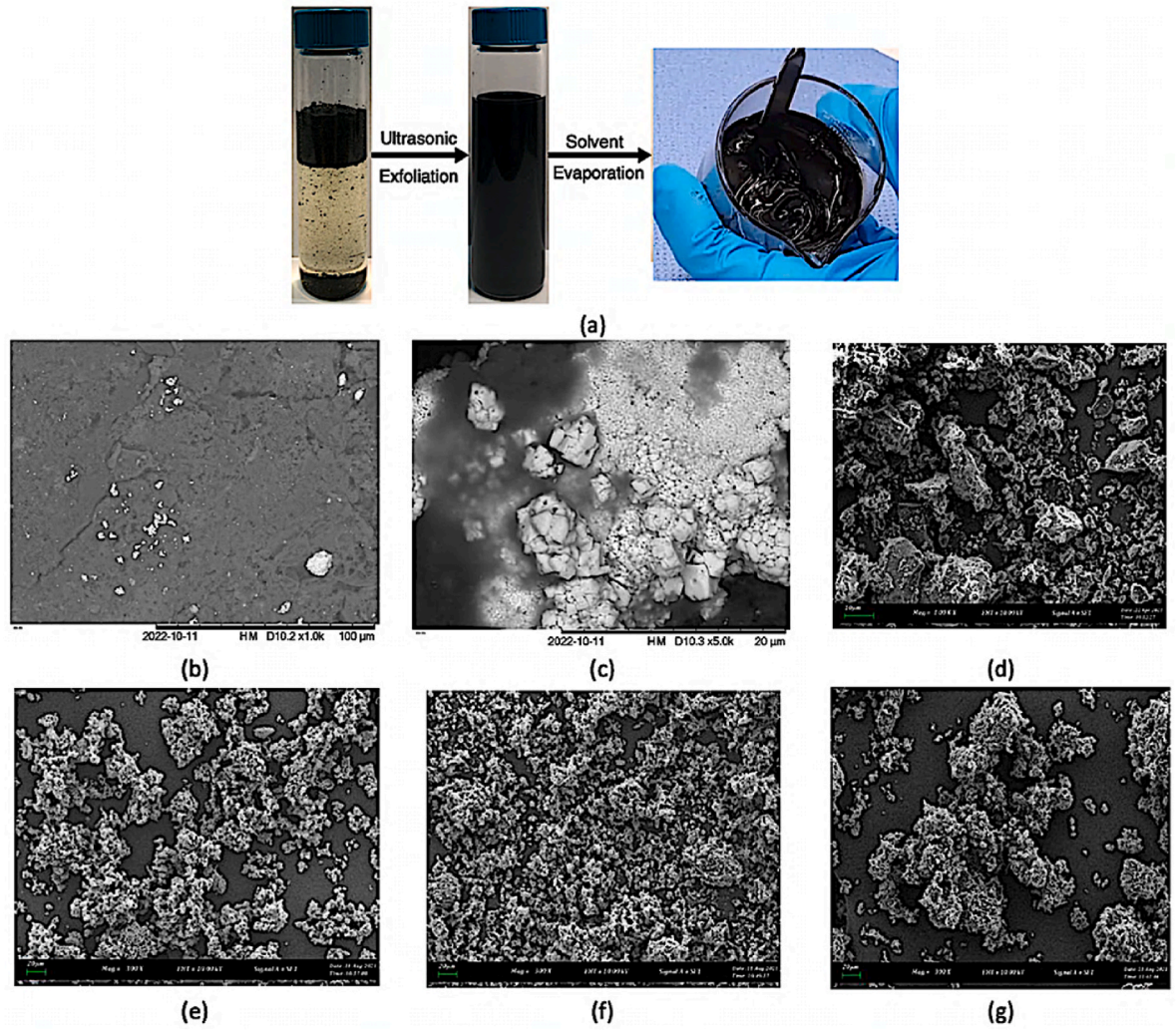

Fig. 2. Morphological representation of GNP/Ag/Cu Conductive Ink: (a) Texture of GNP/Ag/Cu; (b) Low-magnification SEM image showing the overall distribution of constituents; (c) High-magnification SEM image highlighting the morphology of silver particles. SEM micrographs of GNP/Ag/Cu at different concentrations: (d) 0.25 wt% Ag/Cu; (e) 0.50 wt% Ag/Cu; (f) 0.75 wt% Ag/Cu; (g) 1.0 wt% Ag/Cu.

4.20×10^5 S/m and providing enhanced flexibility and processability. The authors in Ref. [30] described a multi-layer graphene film that achieved an electrical conductivity of 2.2×10^5 S/m, developed through ball-milling exfoliation of graphene and subsequent high-temperature annealing. Goulas et al. [31] suggested a microwave metal/ceramic metamaterial antenna structure using metallic silver and silver molybdenum. The ceramic antenna successfully achieved a conductivity of 2×10^6 S/m, and it was noted that the dimensions of the antenna had shrunk by approximately 12.5% after firing. The most recent work done by Wu et al. [32] suggested a graphene folded reflect-array antenna for MM-wave systems. The antenna achieved a high gain of 21.37 dBi at 37.5 GHz, with an electrical conductivity of 7255 S/m.

The issues associated with integrating antennas into textiles, particularly disrupting their inherent softness and lightweight nature, have motivated the development of new material systems. These systems are designed with a profound focus on utilizing two-dimensional materials intelligently within electronic textiles.

This study introduces a groundbreaking superconductive, flexible leather graphene antenna, employing a tri-nanocomposite structure that enhances electrical conductivity and covers a broad bandwidth. By exploring the efficacy of this novel material on fabric and ensuring safety through specific absorption rate testing, the research seeks to advance the capabilities and application of graphene-based inks in wearable electronics.

2. Methodological procedure

The methodology presents a multi-phase process that begins with the creation of a nanocomposite material, as shown in Fig. 1. In Phase 1, the material comprises graphene nanoplatelets (GNP), silver (Ag), and copper (Cu). This composite leverages the high electrical and thermal conductivities of graphene and copper, enhanced by the antimicrobial properties and superior conductivity of silver, which are expected to improve the performance of the final product. The composition includes silver and copper as conductive fillers at concentrations of 0.25 wt percent (wt%), 0.50 wt%, 0.75 wt%, and 1.0 wt%. A consistent temperature and graphene ratio were maintained to develop the GNP/Ag/Cu nanocomposite conductive ink.

Moving into Phase 2, the morphology and electrical conductivity of this nanocomposite are rigorously tested. This is essential to ensure that the material's structure is conducive to electrical applications and that its conductivity meets the requirements for effective signal transmission and reception. For the characterization study, several tests were conducted, including morphological analysis and physical, electrical, and thermal testing. For the morphological evaluation, Scanning Electron Microscopy (SEM) and Energy Dispersive X-ray Analysis (EDS) were employed. Electrical testing was performed on the samples to determine its conductivity characteristics. Comparable to earlier studies, higher conductivity is required to increase the ability to conduct the current

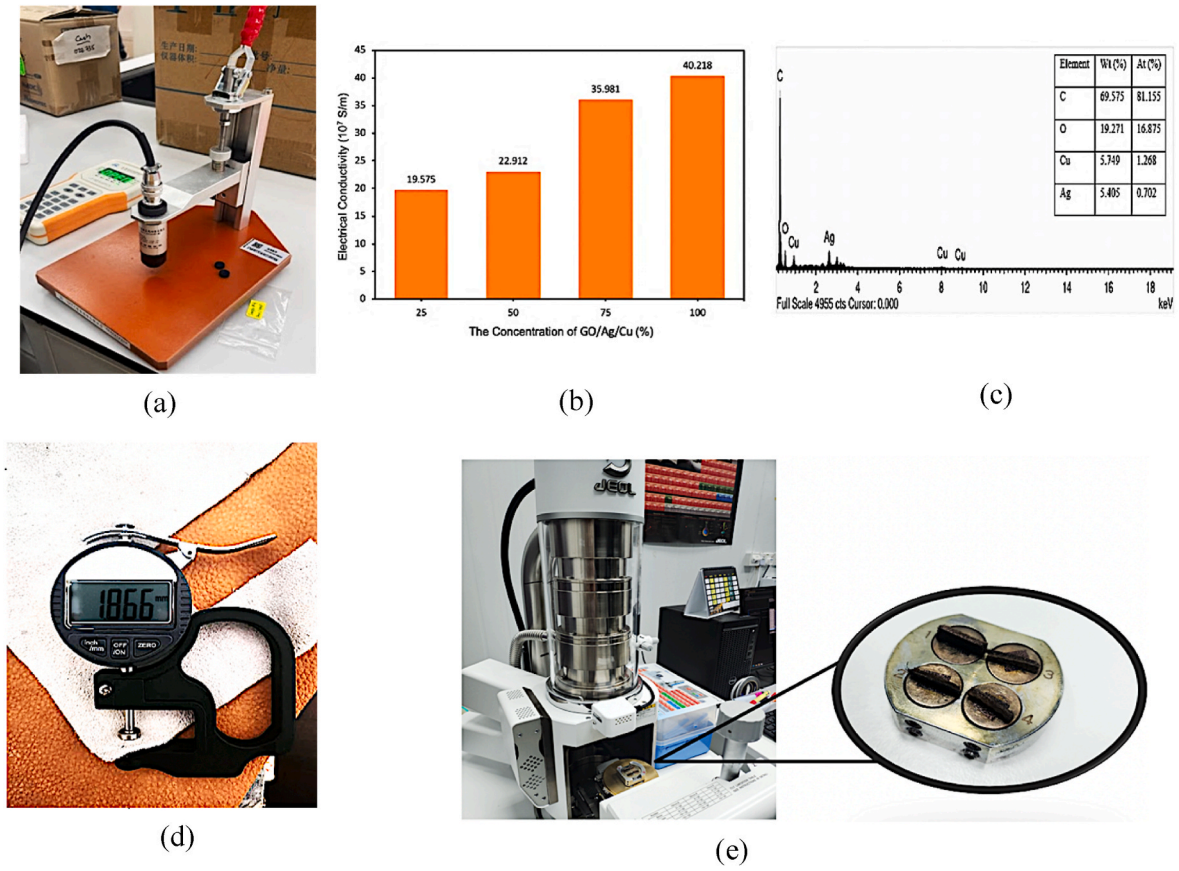

Fig. 3. Conductivity and Thickness Estimation of GNP/Ag/Cu Nanocomposites: (a) Four-point probe measurement; (b) Electrical conductivity of GNP/Ag/Cu nanocomposites; (c) EDX analysis of GNP/Ag/Cu nanocomposites; (d) Leather thickness measurement properties before applying ink, with the following parameters: $\varepsilon_r = 2.2$, tan $\delta = 0.0898$, and thickness = 1.877 mm; (e) Thickness measurement using XRD analysis after applying ink to the surface.

flow.

In Phase 3, the focus shifts to the antenna's design and simulation, utilizing CST Studio Suite 2020 software. The objective is to optimize the antenna's design based on the unique properties of the nanocomposite, ensuring its functionality and efficiency before actual manufacturing.

Phase 4 marks the transition from design to production as the GNP/Ag/Cu nanocomposite is made into conductive ink and printed onto fabrics using a silk-screen printing technique. This phase is critical for integrating the technology into wearable formats, providing flexibility and practicality for the antenna to be used in various applications.

Finally, Phase 5 encompasses the characterization, testing, and analysis of the wearable antenna. It's an exhaustive assessment phase where the antenna is put through its paces in real-world scenarios, its performance meticulously logged and analyzed to confirm it meets the stringent requirements of wearable technology. This method needs to be performed using the silk-screen printing that been adopted as the fabrication process for this proposed selected wearable antenna. Then, the antenna parameters measurement needs to be obtained in order to validate the simulated design as well as the experiment design. These parameters of measurement include reflection coefficient (S11) and gain. Vector network analyzer (VNA) and anechoic chamber are necessary instruments for evaluating the antenna design experimentally.

To assess the impact of the antenna on the human body, it is essential to determine the Specific Absorption Rate (SAR). SAR measures the peak electromagnetic energy deposited in the human body from wireless radiation. Expressed in watts per kilogram (W/kg) or milliwatts per gram (mW/g), SAR values are conventionally averaged over a small mass of tissue, typically 1 and 10 g, in compliance with FCC regulations.

3. Nanocomposite material preparation

A tri-nanocomposite conductive ink of graphene nanoplatelet (GNP) is decorated with silver (Ag) and copper (Cu) has been proposed. The flexible wearable antenna using various type of textile as substrate were fabricated using this conductive nanocomposite. To investigate the morphology and its composition of solution, SEM and EDX analysis were conducted. Meanwhile to test the electrical conductivity, the concept of four-point probe was conducted.

3.1. GNP/Ag/Cu morphology and composition analysis

The tri-nanocomposite ink is produced using graphene nanoplatelets (GNP) through an aniline oxidative polymerization method in an acidic medium, with varied dopant concentrations of silver (Ag) and copper (Cu) at 0.25 wt%, 0.50 wt%, 0.75 wt%, and 1.00 wt%. The optimal composition for the GNP/Ag/Cu conductive ink is at a ratio of 2:1:1. The texture resulting from doping GNP with Ag and Cu is depicted in Fig. 2 (a). This figure illustrates the transformation of graphite into graphene, beginning with ultrasonic exfoliation. Here, graphite particles are subjected to high-frequency sound waves in a vial to produce a dispersion of graphene flakes. Subsequently, the solvent is evaporated to yield a viscous graphene paste, as displayed in the beaker, which is then ready for further applications.

The conductive ink composed of nanocomposites was analyzed in its liquid state using Scanning Electron Microscopy (SEM) for morphological assessment, Energy Dispersive X-ray Analysis (EDX) for elemental composition determination, and a four-point probe test for conductivity measurements. This nanocomposite ink is chemically synthesized from an aqueous mixture containing standard reactants such as aniline,

ammonium persulfate, and sulfuric acid. During the oxidative polymerization of aniline, the solution changes color, eventually forming emerald green precipitates. In SEM analysis, the sample is bombarded with a beam of electrons, prompting the emission of characteristic X-rays from the atoms within the sample. These X-rays' energies and intensities are measured to deduce the elemental composition of the GNP/Ag/Cu sample. Fig. 2(b) and (c) display the surface morphology images. The analyses were conducted at magnifications of 1.0 kx and 5.0 kx, using an accelerating voltage of 15 kV. The surface of the antenna was observed to be uneven, despite the substrate being smooth. This unevenness is typical in screen printing, where the ink is pressed through a mesh, resulting in thinner areas where there are threads.

To evaluate the thickness distribution, measurements were taken at 10 different points across the surface. The average thickness was then calculated from these measurements, providing a single representative value for the overall thickness. These thickness variations can potentially affect the antenna's performance. However, by averaging the measurements from multiple points, we aim to minimize the impact of these variations on the antenna's overall performance.

At 1.0 kx magnification, SEM is utilized to investigate the morphology of GNP/Ag/Cu particles. During doping, silver and copper exhibit a variety of morphologies, including tubes, wires, and particles. GNPs may appear agglomerated and spherical, as depicted in Fig. 2(d). The agglomeration rate of GNPs was higher than that of Ag- and Cu-doped particles, as shown in Fig. 2(d). However, after doping with 0.50 wt% Ag/Cu, the GNPs' structure changed; particle aggregation decreased and became more distinct, as observed in Fig. 2(e). These observations align with previous research, which found that the morphological characteristics of pristine silver and polyurethane (PU) resembled those of GNP. Ag/Cu at 0.25 wt% Ag/Cu loadings, presenting agglomerated globular shapes [33]. With the efficient in situ oxidative polymerization of aniline, the morphological images showed excellent integration of Ag/Cu within the GNP clusters as the Ag/Cu concentration increased to 0.75 wt% and 1.0 wt%, evident in Fig. 2(f) where the morphology appears flaky with various flat and edged surfaces. During in situ polymerization, aniline monomers diffused and polymerized into the graphene nanosheets layer by layer, resulting in the micrographs of GNP/Ag/Cu tri-nanocomposites shown in Fig. 2(g). These findings are corroborated by prior studies indicating flaky morphology with multiple flat and edged surfaces within the graphene cluster following enhanced dispersion with metal materials. Furthermore, the presence of nanocomposite materials is shown to enhance electro-conductivity characteristics due to the networked interlinking between macromolecular clusters.

3.2. Assessing conductivity and thickness of GNP/Ag/Cu for flexible antennas

The electrical conductivity of pressed GNP/Ag/Cu nanocomposite pellets was measured using a four-point probe method. The measurements were conducted with the M − 3 JG square resistance tester and sheet resistance meter from Suzhou Jingge Electronics Co., Ltd., as depicted in Fig. 3(a).

The electrical properties assessed for this sample material include sheet resistivity and conductivity. Equations (1) and (2) were used to calculate the values of resistivity and conductivity, based on the sheet resistivity that was tested [34]:

$$\rho = R_s t \tag{1}$$

The variable ρ represents resistivity in ohms per centimeter (Ω/cm), *Rs* denotes sheet resistance in ohms (Ω), and *t* stands for thickness in centimeters (cm). Meanwhile, the formula for conductivity is as follows [34]:

$$\sigma = \frac{1}{\rho} \tag{2}$$

Whereas σ is Conductivity (S/cm) and ρ is Resistivity (Ω/cm)

The DC conductivity plots of GO/Ag/Cu nanocomposites, measured using the four-point probe technique, are displayed in Fig. 3(b). The data show that lower Ag/Cu concentrations, specifically at 0.25 wt%, result in reduced conductivity compared to higher concentrations. This decrease is attributed to the disturbance in the GNP macromolecular backbone caused by the diminished Ag/Cu levels. Consequently, the reduced Ag/Cu concentrations hinder the formation of complete micelles during aniline polymerization. However, as the concentration of Ag/Cu increases, so do the conductivity values, particularly at higher filler loadings. The presence of Ag/Cu at these higher concentrations accelerates the reaction process by stabilizing and enlarging the GNP micelles, facilitating continuous reaction conditions that enhance conductivity. Additionally, the effective contact between the Ag/Cu flakes improves current transport by reducing resistance among the interlinked particles, thus forming an alternate network channel for current and enhancing electrical conductivity. In this study, GO/Ag/Cu has shown potential as a substitute for traditional materials like copper, silver, graphene, and their composites in wearable antenna applications, due to its superior conductivity of 40.218×10^7 S/m observed in previous research. This enhancement suggests potential improvements for wireless communication applications in the electronics industry, particularly in terms of versatility.

The presence of carbon is the most prominent in the nanocomposite, with an atomic percentage of 81.2% and a concentration of 0.7 wt%, followed by oxygen at 16.9% atomic percentage and 0.2 wt% concentration. Notably, this nanocomposite, identified as GNP/Ag/Cu, also shows detectable signals of silver and copper, constituting 1.3% and 0.7% atomic percentages, respectively, with a concentration of 0.05 wt % for each, as demonstrated in the EDX spectrum shown in Fig. 3(c). Additionally, the tackiness measurement values of the leather textile are presented in Fig. 3(d). The electrical conductivity of the ink used in the printed pattern is significantly influenced by the ink's composition and viscosity, as well as the number of layers applied. To measure the thickness of the conductive ink on the textile, the surface observation and analysis are conducted using a JEOL JSM-IT210 Scanning Electron Microscope. These measurements were performed at magnifications of 1.0 kx and 5.0 kx with an accelerating voltage of 15 kV, as seen in Fig. 3 (e).

Furthermore, SEM has been utilized to measure the thickness of the nanocomposite coating on fabric. Thickness is influenced by several factors, including the type and concentration of filler particles, the matrix material, processing conditions, and performance requirements. Increasing the concentration of filler particles, using thicker matrix materials, or applying multiple layers can enhance the thickness of the coating. This method offers comprehensive insights into the surface morphology, roughness, and thickness of the nanocomposite coating applied to the fabric. It is crucial to consider that the thickness of the nanocomposite coating can also be affected by factors such as the fabric surface, application method, and curing conditions when interpreting measurement results. Additionally, the coating's thickness significantly impacts its performance; therefore, optimizing the thickness to meet the desired performance requirements is essential. The study noted that increasing the number of layers from 5 to 7 only minimally enhances the bandwidth, suggesting that excessive antenna size can be avoided by opting for five layers [35].

The measurement of conductivity ink before printing is approximately 21×10^7 S/m. However, after printing on the leather, the conductivity increases 40.218×10^7 S/m. This significant change is due to the absorption of the ink by the leather. The leather's porosity and surface properties determine how well the conductive ink is absorbed. Better absorption typically leads to a more uniform and continuous conductive path, thereby enhancing conductivity.

With an increase in Ag/Cu concentration, there is a corresponding rise in conductivity values, especially at greater filler loadings. Introducing more Ag/Cu accelerates the reaction process by stabilizing and

Table 1
Summary of the electrical conductivity of various materials used in previous studies compared to our conductive ink.

Previous Studies references	Published Years	Types of material used	Electrical Conductivity (S/m)
[27]	2024	Graphene/Silver	21.3×10^7
[32]	2024	Printed graphene folded reflectarray antenna	7255
[31]	2023	Metal/ceramic metamaterial	2×10^6
[26]	2022	Carbon fiber composite and glass fiber composite	Not proposed
[36]	2022	Graphene coplanar waveguide	3.5×10^5
[38]	2022	Graphene-assembled film	1.1×10^6
[39]	2022	Carbon nanotube film	1×10^5
[37]	2021	Graphene-Assembled Films	1.13×10^6
[41]	2020	Electrifi copper/ Nonconductive NinjaFlex	1.67 × 104
[42]	2018	Copper coated	3.4×10^6
[28]	2018	Graphene film	10^6
[29]	2018	Carbon	4.20×10^5
[30]	2017	Graphene Paper Based on Ball-Milling Exfoliated Graphene	2.2×10^5
This research	**16-May-2024**	**Graphene Nanoplatelet/ Silver/Copper (GNP/Ag/Cu)**	**40.218 x 10^7**

Table 2
Measurement of conductive ink thickness.

Sample	Thickness (mm)
Layer 1	0.135
Layer 2	0.154
Layer 3	0.167
Layer 4	0.169
Layer 5	0.202

expanding the GNP micelles, which leads to sustained reaction conditions that boost conductivity. Furthermore, the improved contact among Ag/Cu flakes facilitates current transport by lowering the resistance between interconnected particles, thus offering an alternative current network channel for enhanced electrical conductivity.

Our conductive ink, composed of Graphene Nanoplatelet/Silver/Copper (GNP/Ag/Cu), exhibits an electrical conductivity of 40.218 × 10^7 S/m. This value is significantly higher than many of the materials used in previous studies, including the Graphene/Silver material with a conductivity of 21.3 × 10^7, and various other composites and films. While compared to the conductive copper as noted in Refs. [41,42], our material's conductivity is much higher than that of pure copper and silver, it still offers significant advantages.

The high conductivity of our ink combined with the flexibility, lightweight nature, and cost-effectiveness makes it a competitive alternative for applications where traditional metals may not be suitable. Furthermore, our material's performance metrics place it among the higher-performing materials in the current landscape of advanced conductive materials, as demonstrated by the comparison in Table 1.

Table 2 shows the measurement of the conductive ink thickness for each layer. By referring to Table 2 and it is evident that there is an incremental increase in thickness layer by layer, from 0.135 mm for the first layer to 0.202 mm for the fifth layer.

There appears to be a consistent increase in thickness with each additional layer. The initial concern regarding the thickness of 4 layers being smaller than the thickness of 3 layers may be due to a typographical error or a misinterpretation. As shown in Table 2 ,the thickness values do increase progressively with each added layer.

Fig. 4 illustrates a cross-section of a leather sample enhanced with a tri-nanocomposite of Graphene Nanoplatelets (GNP), Silver (Ag), and Copper (Cu). The first layer ensures adhesion to the leather, followed by layers that incorporate GNPs for structural strength and conductivity, and metals like silver or copper for added conductivity and antimicrobial properties. The top layer provides environmental and wear protection, collectively enhancing the leather's functionality and durability for specialized uses.

The performance of printing materials with different numbers of

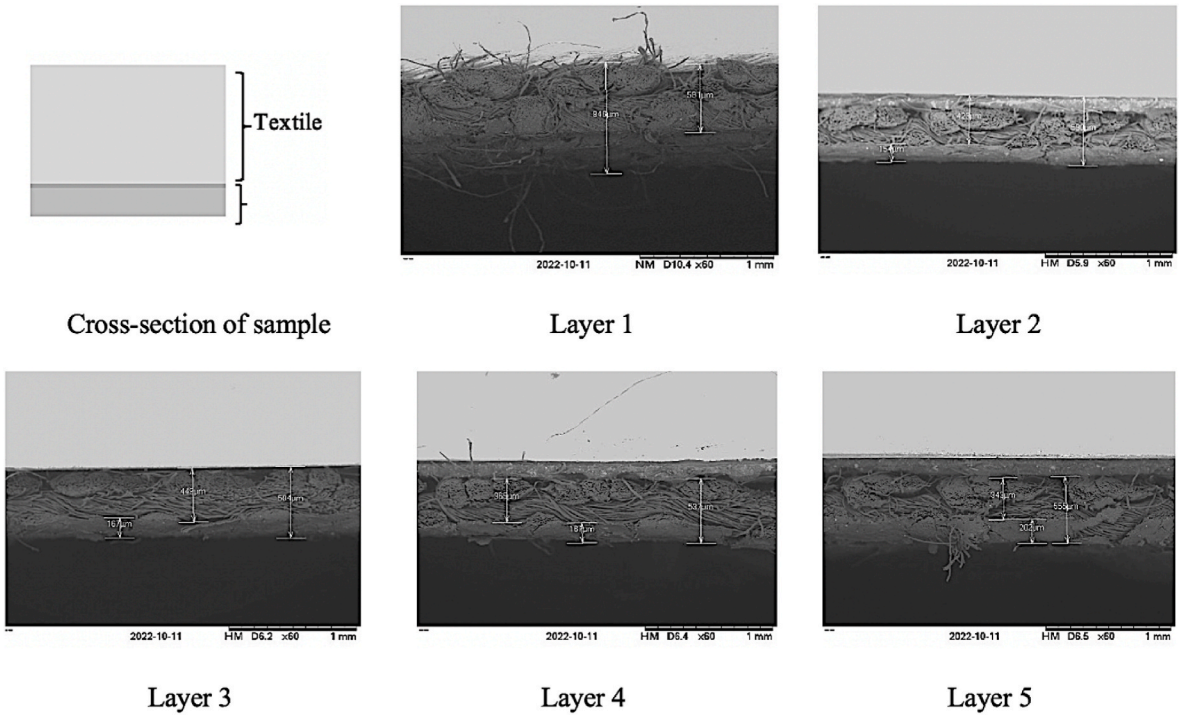

Fig. 4. The thickness of the tri-nanocomposite for different layer of the integration of GNP/Ag/Cu on the leather surface.

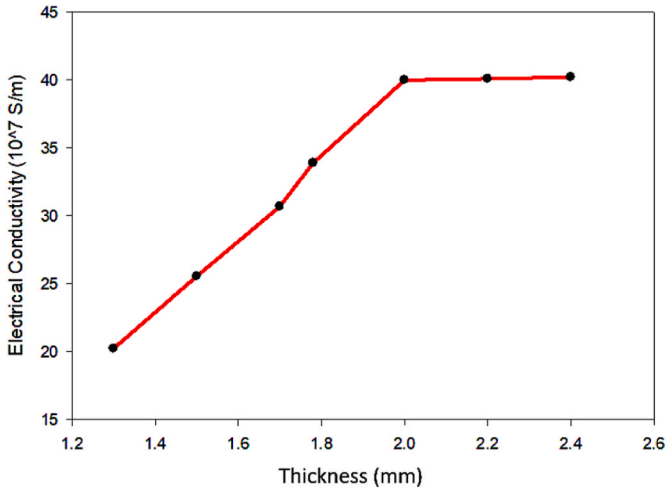

Fig. 5. Electrical Conductivity vs. Thickness for Different Numbers of Layers of GNP/Ag/Cu on the Leather Surface.

layers can vary significantly, particularly in terms of electrical conductivity and mechanical properties such as flexibility. Adding more layers generally increases the overall thickness and conductivity of the printed material due to the increased amount of conductive ink. However, there is a point of diminishing returns where additional layers do not significantly improve performance and can even introduce issues such as increased material cost and potential for defects.

Fig. 5 illustrates the relationship between the number of layers, thickness, and electrical conductivity. As shown, the electrical conductivity increases steadily from the first layer to the fourth layer. However, from the fifth layer onwards, the conductivity plateaus, indicating that additional layers beyond the fifth do not significantly improve conductivity.

As for the electrical conductivity, Fig. 5 demonstrates that a thickness starting from approximately 2.0 mm (corresponding to the fifth to seventh layers) maintains steady electrical conductivity and good flexibility, which is crucial for realizing wearability.

Based on the data presented in Fig. 5 and our experimental findings, we observed that the electrical conductivity increases with the addition of each layer up to the fourth layer. From the fifth layer onwards, the conductivity remains relatively constant, suggesting that the optimal number of layers for maximizing conductivity without unnecessary material usage is around five layers.

The thickness from approximately 2.0 mm (corresponding to the fifth to seventh layers) provides steady electrical conductivity and good flexibility, which is crucial for applications requiring wearability. Additional layers beyond the fifth do not contribute significantly to conductivity but may negatively affect the flexibility and wearability.

To determine the optimal number of layers, we conducted a series of tests, including conductivity measurements using a four-point probe method and flexibility tests to assess the mechanical stability of the printed material under bending and stretching conditions.

4. Fabrication, printing, flexibility and measurements of wearable antennas

The design process, from the antenna design geometry to the fabrication process, has been presented in Fig. 6. The proposed antenna was designed using CST simulation software, employing a leather substrate with a relative permittivity (ε_r) of 2.09 and a tangent loss of 0.0898, with a thickness of 1.866. The modeled antenna consists of three circular rings with different radii dimensions combined for improved antenna impedance matching. A 50-Ω coplanar waveguide (CPW) feedline was used to maintain impedance matching. The geometry, along with the complete dimensions, is presented in Fig. 6(a). The fabrication of the antenna involved silk screen printing, a method commonly used in antenna fabrication for printing conductive ink onto flexible substrates, offering a quick, low-cost, and versatile means to achieve any desired design. The fabrication process of the finalized graphene flexible antenna is detailed as follows: Firstly, the antenna design layout in CST

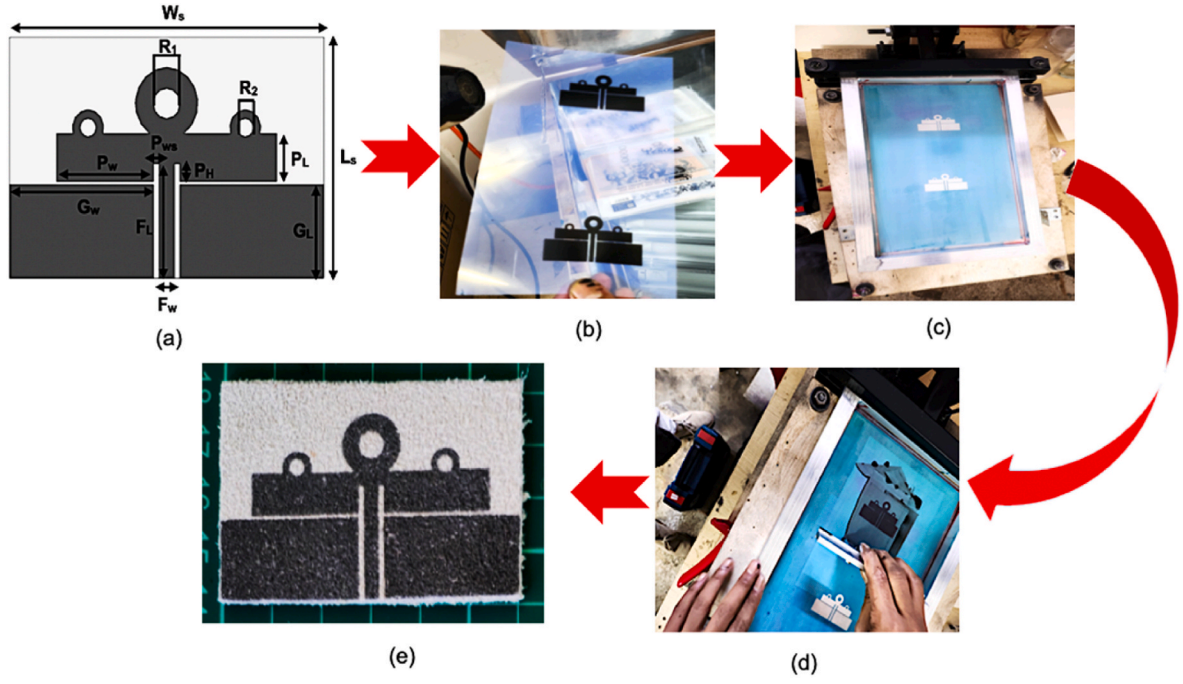

Fig. 6. Representations for the proposed GNP/Ag/Cu antenna from simulation to prototype: (a) Antenna geometry, where $L_s = 40$, $W_s = 60$ $R_1 = 6$, $R_2 = 2.5$, $P_L = 8$, $P_w = 18.5$, $G_L = 15.5$, $G_w = 27.5$, $F_w = 5.16$, $F_L = 19$, $P_H = 3$, $P_{ws} = 1$ (All dimensions are in millimeter (mm)), (b) Printing on Transparency Film with a Laser Jet, (c) Photosensitive emulsion evenly applied to mesh screen, (d) Textiles laid flat; ink applied and spread with a squeegee at 90°, and (e) Fabricated flexible graphene antenna.

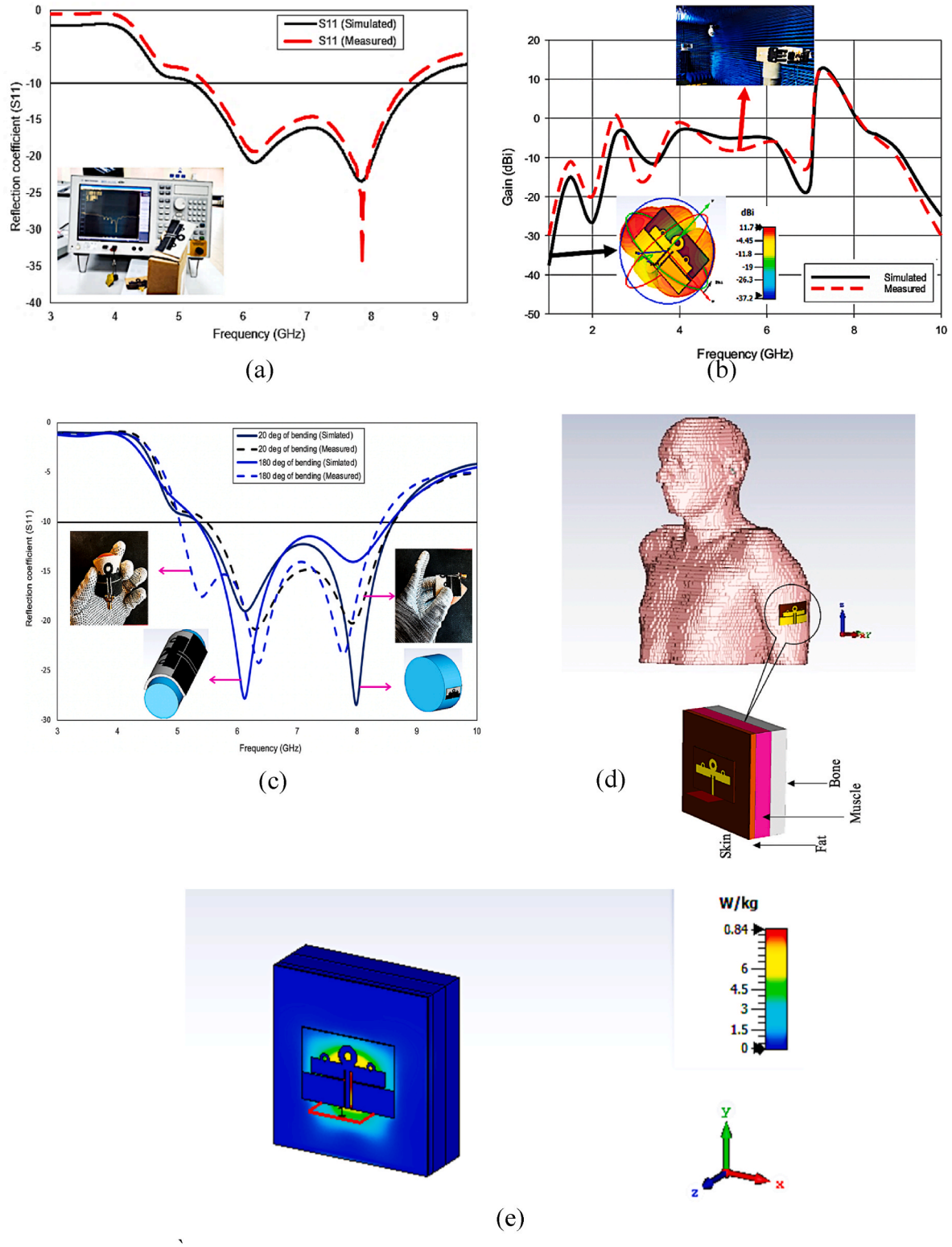

Fig. 7. Illustration of the proposed antenna under various test conditions: (a) Simulated and experimentally measured reflection coefficients (S11), (b) Simulated and actual gain measurements in dBi, (c) Bending analysis at 20° and 180°, (d) Antenna setup on a human body phantom featuring anatomical layers such as skin, fat, muscle, and bone, and (e) SAR values at 7.2 GHz.

software is converted to the drawing format structure using Corel Draw software. Subsequently, the structures are printed onto transparency positive film using a laser jet printer, as depicted in Fig. 6(b), to create the stencil. Next, a coating of photosensitive emulsion is evenly applied to the mesh screen, which hardens upon exposure to bright light. The mesh screen is then dried for several hours in complete darkness due to the emulsion's sensitivity. Following this, the positive film design is laid onto the emulsion-coated screen surface, and the assembly is exposed to intense light, as shown in Fig. 6(c). The light source should be 1 kW, positioned 15 inches above the frame, and exposed for a maximum of 12

Table 3
Characteristics of the human body tissue model.

Parameters	Skin	Fat	Muscle	Bone
Conductivity (S/m)	1.49	0.11	1.77	0.82
Density (kg/m^3)	1001	900	1006	1008
Thickness (mm)	1	5	15	15
Permittivity	37.95	5.27	52.67	18.49

min. Subsequently, the textiles for printing are laid flat underneath the stencil screen. Conductive ink is applied to the top end of the stencil screen, and a squeegee is used at a 90° angle to pull the ink along the complete length of the screen, as illustrated in Fig. 6(d). This process forces ink through the stencil's exposed sections, transferring the design onto the textile beneath, resulting in the designed wearable textile antenna. Finally, the completed antenna prototype is displayed in Fig. 6(e).

The performance of the flexible GNP/Ag/Cu antenna was measured using a Vector Network Analyzer (VNA, Agilent E5071C series). The simulated and measured reflection coefficients (S11) are presented in Fig. 7(a), showing that the measured results align well with the simulated ones. The antenna's bandwidth extends from 5.2 GHz to 8.5 GHz, providing a net bandwidth of 3.3 GHz, which covers the upper band of C-band applications. Optimal impedance matching, at −35 dB, occurs at 7.8 GHz.

The gain of the wearable antenna was measured in an anechoic chamber using signal analyzer equipment. A loss-free isotropic antenna with the same input power Pt_0 would produce this radiation pattern. The proposed flexible antenna achieved a high gain of 12.2 dBi at the resonant frequency of 7.2 GHz as shown in Fig. 7(b). There are slight differences between the simulated and measured gain results due to power reflection at the input array port and dielectric losses.

To analyze the impact of bending on antenna performance in proximity to the human body, the antenna was bent at 20° and 180° along the X- and Y-axes, as shown in Fig. 7(c). The model incorporates varying dielectric properties and conductivity, dependent on the type of human tissues and the frequency involved. Table 3 lists the properties of the human body tissue model values. According to Fig. 7(c), when the antenna is bent at 20°, both the bandwidth and the resonant frequency remain nearly constant, ranging from 5.2 GHz to 8.5 GHz. Conversely, bending the antenna at 180° causes a slight shift toward higher frequencies. This shift occurs because greater bending effectively reduces the antenna's length, thereby raising its resonant frequency. Consequently, the antenna becomes more resonant at these higher frequencies as the shorter effective length better aligns with the corresponding wavelength.

In assessing the antenna's performance with respect to the Specific Absorption Rate (SAR), the influence of the human body on the SAR metric has been considered. Specifications for the human tissue model are detailed in Table 3. A four-layered body phantom, consisting of bone, muscle, fat, and skin, was designed using CST Microwave Studio, as illustrated in Fig. 7(d). The SAR for the flexible GNP/Ag/Cu antenna was simulated at a frequency of 7.2 GHz. SAR quantifies the energy the body absorbs from radio frequency (RF) electromagnetic fields, measured in watts per kilogram of tissue. Unlike typical applications, evaluations of wearable antennas focus on localized rather than whole-body averages. These simulations employed a standard 10 g cubic human tissue model, as depicted in Fig. 7(e). The findings, shown in Fig. 7(e), revealed maximum SAR values of 0.84 W/kg at 7.2 GHz. These SAR levels are well within the safety thresholds of 2 W/kg and 1.6 W/kg established by European and North American standards respectively, as referenced in Ref. [40]. It was also observed that thicker substrates are associated with lower SAR values.

5. Conclusion

This study significantly advances the field of wearable electronics by utilizing a tri-nanocomposite structure of Graphene Nanoplatelet/Silver/Copper (GNP/Ag/Cu) in the development of a superconductive, flexible leather graphene antenna. Demonstrating substantial improvements in conductivity and signal transmission, the antenna effectively covers a bandwidth from 5.2 GHz to 8.5 GHz. Our results show that increasing the layers of GNP/Ag/Cu not only enhances electrical conductivity—from 10.473×10^7 S/m to 40.218×10^7 S/m—but also boosts antenna gain. This enhancement does not sacrifice safety, as evidenced by specific absorption rate (SAR) testing that meets ICNIRP standards, registering 0.84 W/kg per 10 g of tissue at 0.5 W input power. Further, morphological analyses highlight the antenna's robustness and adaptability for integration into everyday wearable devices. By overcoming the challenges associated with graphene's inherent properties, this research paves the way for future innovations in printable electronics on flexible materials, offering more accessible, efficient, and eco-friendly solutions in wearable technology.

CRediT authorship contribution statement

Ahmed Jamal Abdullah Al-Gburi: Writing – original draft, Project administration. **Nor Hadzfizah Mohd Radi:** Software, Methodology. **Tale Saeidi:** Investigation, Formal analysis. **Naba Jasim Mohammed:** Formal analysis, Data curation. **Zahriladha Zakaria:** Validation, Supervision. **Gouree Shankar Das:** Resources, Conceptualization. **Akash Buragohain:** Software, Methodology. **Mohd Muzafar Ismail:** Writing – review & editing, Project administration.

Declaration of competing interest

The authors declare that they have no known competing financial interests or personal relationships that could have appeared to influence the work reported in this paper.

Acknowledgements

The authors express their thank and acknowledge the support from Universiti Teknikal Malaysia Melaka (UTeM), the Centre for Research and Innovation Management (CRIM), and the Ministry of Higher Education of Malaysia (MOHE). Additionally, the authors are also thankful to Universiti Malaysia Pahang Al-Sultan Abdullah for their support.

References

[1] S. Chung, K. Cho, T. Lee, Recent progress in inkjet-printed thin-film transistors, Adv. Sci. 6 (6) (2019).
[2] J.V. Vaghasiya, C.C. Mayorga-Martinez, M. Pumera, Wearable sensors for telehealth based on emerging materials and nanoarchitectonics, NPJ Flex. Electron. 7 (2023) 26.
[3] K. Pan, Y. Fan, T. Leng, et al., Sustainable production of highly conductive multilayer graphene ink for wireless connectivity and IoT applications, Nat. Commun. 9 (2018) 5197, https://doi.org/10.1038/s41467-018-07632-w.
[4] S. Zhang, J. Zhu, Y. Zhang, Z. Chen, C. Song, J. Li, N. Yi, D. Qiu, K. Guo, C. Zhang, T. Pan, Y. Lin, H. Zhou, H. Long, H. Yang, H. Cheng, Standalone stretchable RF systems based on asymmetric 3D microstrip antennas with on-body wireless communication and energy harvesting, Nano Energy 96 (2022), https://doi.org/10.1016/j.nanoen.2022.107069107069.
[5] L. Zhou, Y. Tian, P. Xu, H. Wei, Y. Li, H.X. Peng, F. Qin, Effect of the selective localization of carbon nanotubes and phase domain in immiscible blends on tunable microwave dielectric properties, Compos. Sci. Technol. 213 (2021) 108919, https://doi.org/10.1016/j.compscitech.2021.108919.
[6] Y.Z.N. Htwe, M. Mariatti, Printed graphene and hybrid conductive inks for flexible, stretchable, and wearable electronics: progress, opportunities, and challenges, J. Sci. Adv. Mater. Devices 7 (2022) 100–435.
[7] I. Ibanez-Labiano, M.S. Ergoktas, C. Kocabas, A. Toomey, A. Alomainy, E. Ozden-Yenigun, Graphene-based soft wearable antennas, Appl. Mater. Today 20 (2020) 100727.
[8] F. Ruiz-Perez, S. López-Estrada, R. Tolentino-Hernández, F.J.J. Caballero-Briones, And Devices, "Carbon-based radar absorbing materials: a critical review,", J. Sci. Adv. Mater. Devices 7 (3) (2022) 100454.
[9] N. Ibrahim, J.O. Akindoyo, M. Mariatti, Recent development in silver-based ink for flexible electronics, J. Sci. Adv. Mater. Devices 7 (2022), https://doi.org/10.1016/j.jsamd.2021.09.002.

[10] R.K. Baruah, H. Yoo, E.K. Lee, Interconnection technologies for flexible electronics: materials, fabrications, and applications, Micromachines 14 (2023) 1131, https://doi.org/10.3390/mi14061131.
[11] Z. Li, Y. Gong, D. Zhao, Z. Dang, Z. Lin, Enhanced removal of zinc and cadmium from water using carboxymethyl cellulose-bridged chlorapatite nanoparticles, Chemosphere 263 (2021), https://doi.org/10.1016/j.chemosphere.2020.128038.
[12] A. Kamyshny, S. Magdassi, Conductive nanomaterials for printed electronics, Small 10 (2014) 3515–3535.
[13] C.-Y. Lo, Y. Zhao, C. Kim, Y. Alsaid, R. Khodambashi, M. Peet, R. Fisher, H. Marvi, S. Berman, D. Aukes, X. He, Highly stretchable self-sensing actuator based on conductive photothermally-responsive hydrogel, Mater. Today 50 (2021) 35–43, https://doi.org/10.1016/j.mattod.2021.05.008.
[14] M. Terrones, Science and technology of the twenty first century: synthesis, properties, and applications of carbon nanotubes, Ann Rev Mater Res 33 (2003) 419–501.
[15] Peter S. Hall, Antennas and Propagation for Body-Centric Wireless Communications, second ed., 9781608073764 (Book).
[16] R. Lin, H.J. Kim, S. Achavananthadith, et al., Digitally-embroidered liquid metal electronic textiles for wearable wireless systems, Nat. Commun. 13 (2022) 2190, https://doi.org/10.1038/s41467-022-29859-4.
[17] M. El Gharbi, R. Fernández-García, I. Gil, Embroidered wearable antenna-based sensor for real-time breath monitoring, Measurement 195 (2022) 111080, https://doi.org/10.1016/j.measurement.2022.111080.
[18] F.R. Kareem, M. El Atrash, A.A. Ibrahim, M.A. Abdalla, All-textile inspired-folded dipole antennas for on/off-body communications medical applications, Alexandria Eng J 61 (11) (2022) 8751–8761, https://doi.org/10.1016/j.aej.2022.02.026.
[19] R. Muthu Krishnan, G. Kannan, A compact dual-sense circularly polarized SIW textile antenna for body-centric wireless communication, AEU-International Journal of Electronics and Communications (2023) 154523.
[20] Z. He, Y. Wang, H. Xiao, Y. Wu, X. Xia, S. Li, J. Liu, K. Huang, F. Wang, J. Shang, Y. Liu, H. Li, F. Li, S. Wang, G. Zhu, R.-W. Li, Highly stretchable, deformationstable wireless powering antenna for wearable electronics, Nano Energy 112 (2023) 108461, https://doi.org/10.1016/j.nanoen.2023.108461.
[21] S. Ahmad, H. Boubakar, S. Naseer, M.E. Alim, Y.A. Sheikh, A. Ghaffar, A.J. A. AlGburi, N.O. Parchin, Design of a tri-band wearable antenna for millimeter-wave 5G applications, Sensors 22 (2022), https://doi.org/10.3390/s22208012.
[22] H.F. Abutarboush, Silver nanoparticle inkjet-printed multiband antenna on synthetic paper material for flexible devices, Alex. Eng. J. 61 (8) (2022) 6349–6355, https://doi.org/10.1016/J.AEJ.2021.11.060.
[23] S.B. Roshni, S. Arun, M.T. Sebastian, P. Mohanan, K.P. Surendran, Low κ Mg2SiO4 ceramic tapes and their role as screen printed microstrip patch antenna substrates, Mater. Sci. Eng. B 264 (2021) 114947, https://doi.org/10.1016/j.
[24] M.T. Gatte, P.J. Soh, R.A. Kadhim, H.J. Abd, R.B. Ahmad, Modeling and performance evaluation of antennas coated using monolayer graphene in the millimeter and sub-millimeter wave bands, Int. J. Numer. Model. Electron. Network. Dev. Field. 34 (5) (2021) 1–12, https://doi.org/10.1002/jnm.2929.
[25] H.J. Kwon, J. Hong, S.Y. Nam, H.H. Choi, X. Li, Y.J. Jeong, S.H. Kim, Overview of recent progress in electrohydrodynamic jet printing in practical printed electronics: focus on the variety of printable materials for each component, Mater. Adv. 2 (2021) 5593–5615.
[26] X. Guo, S. Lin, F. Dai, A metal hybrid bistable composite tube for multifunctional and reconfigurable antenna, Compos. Sci. Technol. 233 (2023) 109887.
[27] A.J.A. Al-Gburi, M.M. Ismail, N.J. Mohammed, A. Buragohain, K. Alhassoon, Electrical conductivity and morphological observation of hybrid filler: silver-graphene oxide nanocomposites for wearable antenna, Opt. Mater. 148 (2024) 114882.
[28] D. Tang, Q. Wang, Z. Wang, Q. Liu, B. Zhang, D. He, Z. Wu, S. Mu, Highly sensitive wearable sensor based on a flexible multi-layer graphene film antenna, Sci. Bull. 63 (2018) 574–579.
[29] A. Scidà, et al., Application of graphene-based flexible antennas in consumer electronic devices, Mater. Today 21 (3) (2018) 223–230, https://doi.org/10.1016/j.mattod.2018.01.007.
[30] C. Teng, D. Xie, J. Wang, et al., Ultrahigh conductive graphene paper based on ball-milling exfoliated graphene, Adv. Funct. Mater. 27 (2017) 1700240.
[31] A. Goulas, T. Whittaker, G. Chi-Tangyie, I.M. Reaney, D.S. Engstrøm, W. G. Whittow, Bala Vaidhyanathan, Multi-material additive manufacture and microwave-assisted sintering of a metal/ceramic metamaterial antenna structure, Appl. Mater. Today 33 (2023), https://doi.org/10.1016/j.apmt.2023.101878,101878-101878.
[32] Qiyun Wu, Yuwei Xiong, Yizhu Shen, Song Xue, Kuibo Yin, Litao Sun, Laser-Assisted screen-printing of graphene folded reflectarray antenna for millimeter-wave applications, Carbon (2024) 119235, https://doi.org/10.1016/j.carbon.2024.119235.
[33] D. Suh, D.W. Kim, P. Liu, H. Kim, J.A. Weninger, C.M. Kumar, A. Prasad, B. W. Grimsley, H.B. Tejada, Effects of Ag content on fracture resistance of Sn–Ag–Cu lead-free solders under high-strain rate conditions, Mater. Sci. Eng. B 460–461 (2007) 595–603.
[34] I. Miccoli, F. Edler, H. Pfnür, C. Tegenkamp, The 100th anniversary of the four-point probe technique: the role of probe geometries in isotropic and anisotropic systems, J. Phys. Condens. Matter 27 (2015) 223201.
[35] F. Khajeh-Khalili, A. Shahriari, F. Haghshenas, A simple method to simultaneously increase the gain and bandwidth of wearable antennas for application in medical/communications systems, International Journal of Microwave and Wireless Technologies 13 (4) (2021) 374–380, https://doi.org/10.1017/S1759078720001075.
[36] N. Morales-Centla, R. Torrealba-Melendez, E.I. Tamariz-Flores, M. López-López, C. A. Arriaga-Arriaga, J.M. Munoz-Pacheco, V.R. Gonzalez-Diaz, Dual-band CPW graphene antenna for smart cities and IoT applications, Sensors 22 (2022) 5634, https://doi.org/10.3390/s22155634.
[37] Z. Hu, Z. Xiao, S. Jiang, R. Song, D. He, A dual-band conformal antenna based on highly conductive graphene-assembled films for 5G WLAN applications, Materials 14 (2021) 5087, https://doi.org/10.3390/ma14175087.
[38] S. Jiang, R. Song, Z. Hu, Y. Xin, G.L. Huang, D. He, Millimeter wave phased array antenna based on highly conductive graphene-assembled film for 5G applications, Carbon 196 (2022) 493–498.
[39] H. Song, H. Jeon, D. Im, N. Çakmakçı, K.-Y. Shin, Y. Jeong, Free-standing carbon nanotube film for high efficiency monopole antenna, Carbon N Y 187 (2022) 22–28, https://doi.org/10.1016/j.carbon.2021.10.068.
[40] N. Mukherjee, A. Kundu, B. Gupta, M. Mitra, Specific absorption rate estimation for a typical Hibiscus flower model as per ICNIRP electromagnetic guidelines. 2020 *IEEE Calcutta Conference (CALCON)*, 2020, pp. 240–243, https://doi.org/10.1109/CALCON49167.2020.9106570. Kolkata, India.
[41] D. Mitra, S. Roy, R. Striker, E. Burczek, A. Aqueeb, H. Wolf, et al., Conductive electrifi and nonconductive NinjaFlex filaments based flexible microstrip antenna for changing conformal surface applications, Electronics 10 (7) (Mar. 2021) 821.
[42] R.B.V.B. Simorangkir, Y. Yang, R.M. Hashmi, T. Björninen, K.P. Esselle, L. Ukkonen, Polydimethylsiloxane-embedded con- ductive fabric: characterization and application for realization of robust passive and active flexible wearable antennas, IEEE Access 6 (2018) 48102–48112.